

# Nanocrystallization process in Finemet-type alloys followed by in situ $^{57}\text{Fe}$ Mössbauer spectroscopy

V.A. Peña Rodríguez<sup>a,\*</sup>, J. Flores Regalado<sup>a</sup>, E. Baggio-Saitovitch<sup>b</sup>, E.C. Passamani<sup>c</sup>

<sup>a</sup> Facultad de Ciencias Físicas, Universidad Nacional Mayor de San Marcos, P.O. Box 14-149, Lima 14, Peru

<sup>b</sup> Centro Brasileiro de Pesquisas Físicas, Rua Dr. Xavier Sigaud 150, Urca, CEP 22290-180 Rio de Janeiro, Brazil

<sup>c</sup> Departamento de Física, Universidade Federal de Espírito Santo, Vitória, CEP 29060-900 Espírito Santo, Brazil

Received 19 December 2003; received in revised form 16 February 2004; accepted 16 February 2004

## Abstract

High-temperature in situ  $^{57}\text{Fe}$  Mössbauer spectroscopy was used to investigate the nanocrystallization process in  $\text{Fe}_{73.5}\text{Si}_{13.5}\text{B}_9\text{Cu}_1\text{Nb}_1\text{X}_2$  ( $\text{X} = \text{Zr}, \text{Nb}, \text{Mo}$  and  $\text{V}$ ) amorphous alloys. The Mössbauer spectra were taken at temperatures where only the amorphous phase is found in a paramagnetic state, allowing an accurate resolution between the amorphous and crystalline phases presented in the annealed ribbons. The Johnson–Mehl–Avrami theory was used to describe the increase of the crystalline fraction (in vol.%) as a function of the annealing time. The volume fraction of the iron-silicate nanocrystalline phase, found in each of the alloys annealed under similar conditions, increases in the sequence  $\text{Zr} < \text{Nb} < \text{Mo} < \text{V}$ . The value of the Avrami exponent, determined for each alloy, is near 1, indicating a controlled diffusion process with a nucleation rate close to zero. An activation energy of 3 eV was found for the studied alloys.

© 2004 Elsevier B.V. All rights reserved.

**Keywords:** Nanostructures; Magnetically ordered materials; Clusters; Amorphous materials; Mössbauer spectroscopy

## 1. Introduction

Iron-based nanocrystalline alloys, obtained after appropriate heat treatment of an amorphous precursor, consist primarily of iron-silicate crystals embedded in an amorphous residual matrix. The grain size of iron-silicate particles is in the range of 5–20 nm in diameter. The formation and the thermal stability of the iron-silicate phase are attributed to the effect of Cu as well as the refractory elements, such as Nb, Zr, Mo and V. Cu enhances the nucleation frequency, while the refractory elements can slow down the grain growth rate [1–4]. Therefore, one of the aims of the present work is to gain an insight into the kinetics of the nanocrystallization, in order to better understand the role of refractory elements in inhibiting the growth of the iron-silicate phase.

Iron nuclides are very sensitive to changes in the local neighborhood created during the annealing process. Therefore, high-temperature in situ  $^{57}\text{Fe}$  Mössbauer spectroscopy is a suitable technique to investigate the kinetics of the phase

transformation and the crystallization process in iron-based amorphous materials. For example, with the Mössbauer method one is able to follow the growth of different phases as well as to determine their relative contents produced during the annealing of an amorphous alloy, leading to a better understanding of the kinetic phenomena. However, in Si-bearing nanocrystalline Finemet-type alloys, the complexity of the hyperfine structure of the Mössbauer spectra prevents an immediate and accurate analysis. Indeed, as it will be shown below, the Mössbauer spectra show multiple narrow lines, which represent structurally different crystallographic sites assigned to the iron-silicate grains, superimposed on a broadened feature ascribed to the residual amorphous phase. One of the main difficulties in the fitting procedure is to accurately separate the amorphous and crystalline components, which are strongly overlapped at room temperature. The validity of the fitting model also needs to be controlled to prevent misinterpretations [5]. In situ  $^{57}\text{Fe}$  Mössbauer measurements at temperatures above the Curie temperature ( $T_C$ ) of the amorphous sample [6] permit better resolution of the two observed components, i.e., the crystalline component is magnetically ordered at temperatures not too far above  $T_C$  of the amorphous phase

\* Corresponding author.

E-mail address: vpenar@unmsm.edu.pe (V.A. Peña Rodríguez).

Table 1

Crystallization onset temperature,  $T_{\text{onset}}$ , and kinetic parameters for different annealing temperatures,  $T_a$ : incubation time,  $t_{\text{inc}}$ , rate constant,  $k$ , Avrami index,  $n$ , and saturation value of the crystalline fraction,  $x_{\text{sat}}$ , for  $\text{Fe}_{73}\text{Si}_{13.5}\text{B}_9\text{Cu}_1\text{Nb}_1\text{X}_2$  ( $\text{X} = \text{Zr}, \text{Nb}, \text{Mo}$  and  $\text{V}$ ) nanocrystalline alloys

X	$T_{\text{onset}}$ (K)	$T_a$ (K)	$t_{\text{inc}}$ (s)	$k$ ( $\times 10^{-4} \text{ s}^{-n}$ ) ( $\pm 0.5$ )	$n$ ( $\pm 0.1$ )	$x_{\text{sat}}$ (%) ( $\pm 3$ )
Zr	797	797	500	1.1	1.0	51
		813	300	2.0	1.0	57
Nb	791	797	400	1.5	1.0	53
		807	300	2.1	1.0	57
Mo	772	741	800	1.1	1.1	48
		756	650	1.4	1.0	50
V	763	733	800	1.1	1.1	48
		769	400	1.8	1.0	53

(amorphous phase found in the paramagnetic state). Thus, the amorphous subspectrum can be associated with a central paramagnetic doublet, while the iron-silicate contributes to the magnetic subspectra at temperatures slightly higher than  $T_C$  of the amorphous phase.

The present work examines the influence of refractory element substitution on the nanocrystallization kinetics of  $\text{FeSiBCuNb}$ -based amorphous alloys using high-temperature in situ  $^{57}\text{Fe}$  Mössbauer measurements. The obtained results will be correlated with those previously reported on the crystallization process and transformation kinetics of these alloys by differential scanning calorimetry, electron microscopy, X-ray diffraction and EXAFS spectroscopy [7–9].

## 2. Experimental

$\text{Fe}_{73.5}\text{Si}_{13.5}\text{B}_9\text{Cu}_1\text{Nb}_1\text{X}_2$  ( $\text{X} = \text{Zr}, \text{Nb}, \text{Mo}$  and  $\text{V}$ ) amorphous ribbons were first quenched from master alloys by a melt-spinning technique at the Polytechnical University of Warsaw. The ribbon thicknesses are in the range of 1–3 mm. Slabs of 1.5 cm  $\times$  1.5 cm from the ribbon alloys were cut for Mössbauer analysis.

Isothermal treatments of 240 min in a vacuum Mössbauer furnace ( $\sim 10^{-6}$  mbar) were performed for all alloys, at temperatures close to the crystallization onset ( $T_{\text{onset}}$ ) of each alloy determined by DSC (Table 1 [7]). In continuous isothermal annealing, in situ Mössbauer spectra were recorded during 20 min using a transmission geometry with a 25 mCi  $^{57}\text{Co}:\text{Rh}$  source kept at 300 K. In this experimental geometry, the  $\gamma$ -ray direction is perpendicular to the ribbon plane. The spectra were fitted using the NORMOS program [10].

Mössbauer spectra of the as-quenched alloys were fitted using a distribution of hyperfine parameters, consistent with an amorphous structure. In order to reproduce the asymmetrical shape of the Mössbauer spectra, it was necessary to introduce a linear correlation between the magnetic hyperfine field and the isomer shift [11], although it should be noted that this linear relationship has no physical meaning.

The spectra of the annealed samples exhibit a complex hyperfine structure in which sharp lines produced by the crystalline phase are superimposed on the broad overlapping lines associated with a residual amorphous matrix. The contribution to the spectra corresponding to the iron-silicate phase, with a  $\text{DO}_3$  structure, was fitted assuming a set of five sextets, corresponding to different number of Fe and Si atoms as nearest-neighbors of the Fe atoms. The amorphous components observed in the spectra of different samples, taken at room temperature, were fitted to magnetic field distributions, while in the case of spectra taken in the temperature range from 733 to 813 K, asymmetric electric quadrupolar doublets were used, since the amorphous phases are found in the paramagnetic state at these temperatures.

## 3. Results and discussion

Fig. 1 shows the transmission Mössbauer spectra of the  $\text{Fe}_{73.5}\text{Si}_{13.5}\text{B}_9\text{Cu}_1\text{Nb}_1\text{Mo}_2$  alloys. Plot (b) corresponds to

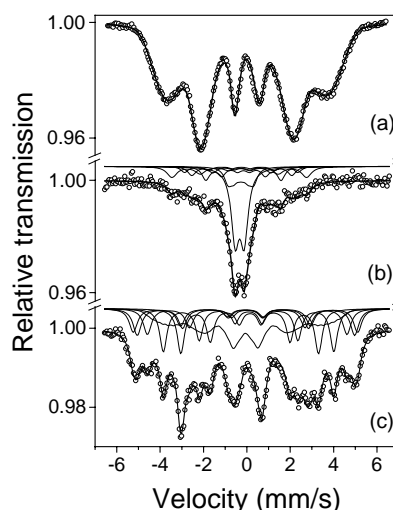


Fig. 1.  $^{57}\text{Fe}$  Mössbauer spectra of the  $\text{Fe}_{73.5}\text{Si}_{13.5}\text{B}_9\text{Cu}_1\text{Nb}_1\text{Mo}_2$  alloy: as-quenched at 300 K (a) and annealed and measured at 756 K for 240 min (b); and the same sample used for (b) after being cooled down to 300 K (c).

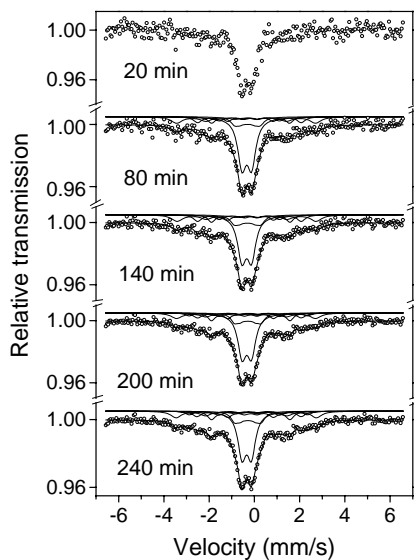


Fig. 2. In situ  $^{57}\text{Fe}$  Mössbauer spectra of the  $\text{Fe}_{73.5}\text{Si}_{13.5}\text{B}_9\text{Cu}_1\text{Nb}_1\text{Mo}_2$  alloy recorded at 756 K during isothermal annealing for different times.

the spectrum obtained after isothermal annealing of this sample at 756 K for 240 min. For comparison, plots (a) and (c) display the Mössbauer spectra for the as-quenched and the annealed samples, after cooling down the sample (plot (b)) to room temperature.

As discussed in Section 2, the fits of these spectra were done using one component associated with the amorphous phase (magnetic distribution for plot 1a or doublet for high-temperature spectrum) and a set of sextets attributed to the  $\text{DO}_3$  structure of the iron-silicate phase (plots (b) and (c) of Fig. 1). Also for all the as-quenched alloys, the orientation of Fe magnetic moments was calculated from the ratio of the respective line intensities given by  $3:x:1:1:x:3$  with  $x = 4 \sin^2(\theta)/(1 + \cos^2(\theta))$ , where  $\theta$  being the angle between the incident  $\gamma$ -ray and the direction of the magnetization. As the incident photon direction is along the normal of the sample surface one should observe 3:4:1:1:4:3 for in-plane magnetization, whereas out-of-plane results in 3:0:1:1:0:3. In as-quenched samples, the relative line intensity from the spectrum indicates that the magnetization of the Fe atoms is in the ribbon planes for Nb-, Mo- and V-containing systems, while isotropic magnetic domains is observed for Zr-based alloy.

Fig. 2 shows the time dependence of the Mössbauer spectra for the  $\text{Fe}_{73.5}\text{Si}_{13.5}\text{B}_9\text{Cu}_1\text{Nb}_1\text{Mo}_2$  alloy recorded during isothermal annealing at 756 K. All spectra are composed of a central doublet, associated with the amorphous phase in the paramagnetic state, superimposed on a broad magnetic subspectrum attributed to the  $\text{DO}_3$  structure of the iron-silicate phase. From this figure, it can be seen that the relative absorption area of the amorphous subspectrum (doublet) decreases with the increase of annealing time. On the other hand, this effect corresponds to an increase in the volume fraction of the iron-silicate nanocrystalline phase due to the crystallization process that is in progress.

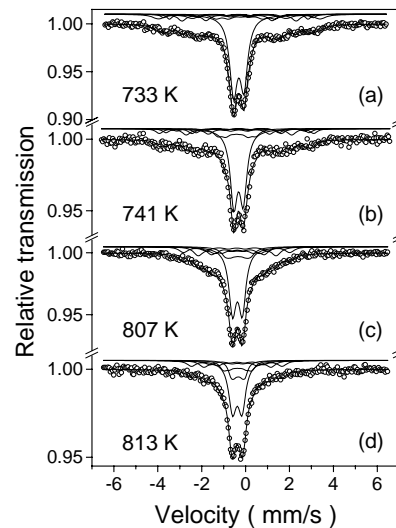


Fig. 3. In situ  $^{57}\text{Fe}$  Mössbauer spectra of the  $\text{Fe}_{73.5}\text{Si}_{13.5}\text{B}_9\text{Cu}_1\text{Nb}_1\text{X}_2$  alloys annealed at indicated temperatures for 240 min: X = V (a), X = Mo (b), X = Nb (c) and X = Zr (d).

For comparison, Fig. 3 shows displayed the high-temperature in situ Mössbauer spectra for the  $\text{Fe}_{73.5}\text{Si}_{13.5}\text{B}_9\text{Cu}_1\text{Nb}_1\text{X}_2$  (X = V, Mo, Nb and Zr) nanocrystalline alloys submitted to heat treatments under similar conditions, for a period of 240 min at 733, 741, 807 and 813 K, respectively.

These temperatures correspond to the onset temperatures minus 30 K ( $T_{\text{onset}} - 30\text{ K}$ ) for the V- and Mo-containing alloys and onset temperatures plus 16 K ( $T_{\text{onset}} + 16\text{ K}$ ) for the alloys with X = Nb and Zr. As can be seen the spectra have also two distinct components: the doublet associated with the amorphous phase in paramagnetic states and a set of sextets attributed to the iron-silicate phase. The volume of the crystalline fractions of the iron-silicate phase, obtained from the fittings of the Mössbauer spectra recorded after the isothermal treatment, for 240 min are roughly 44% for the alloys annealed at  $T_{\text{onset}} - 30\text{ K}$  (Mo- and V-based alloys) and about 53% for the alloys annealed at  $T_{\text{onset}} + 16\text{ K}$  (Zr- and Nb-based alloys), regardless of the composition.

Fig. 4 shows the dependence of the iron-silicate phase volume fractions of the  $\text{Fe}_{73.5}\text{Si}_{13.5}\text{B}_9\text{Cu}_1\text{Nb}_1\text{X}_2$  nanocrystalline alloys obtained as a function of annealing time, for isothermal treatment at: (a)  $T_{\text{onset}} + 16\text{ K}$ , (b)  $T_{\text{onset}} + 6\text{ K}$  and (c)  $T_{\text{onset}} - 30\text{ K}$ . For all curves in this figure, it is observed that the iron-silicate phase crystalline fraction volume increases monotonously with annealing time up to a saturation value, which depends on the annealing temperature ( $T_{\text{ann}}$ ). The corresponding curves at the same  $\Delta T (= T_{\text{ann}} - T_{\text{onset}})$ , below or above the respective crystallization onset temperature of each alloy, are superimposed. In terms of the crystalline fractions, this feature might indicate that the only difference in the behavior of these studied alloys is the stability of the amorphous alloys precursor against nanocrystallization. Similar results were obtained from in situ X-ray diffraction measurements using a synchrotron radiation source [8].

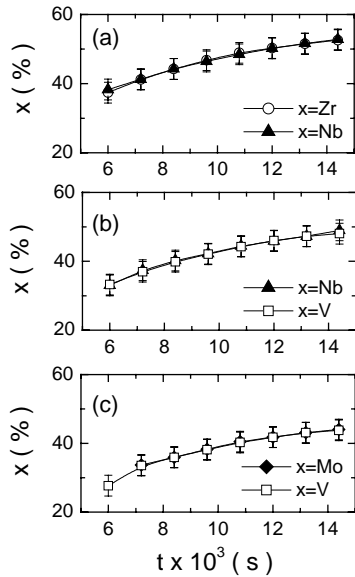


Fig. 4. Dependence of the iron-silicate fraction obtained in  $\text{Fe}_{73.5}\text{Si}_{13.5}\text{B}_9\text{Cu}_1\text{Nb}_1\text{X}_2$  nanocrystalline alloys as a function of annealing time performed at constant temperatures of: (a)  $T_{\text{onset}} + 16$  K, (b)  $T_{\text{onset}} + 6$  K and (c)  $T_{\text{onset}} - 30$  K.

The time dependence of the crystalline volume fraction was described in terms of the Johnson–Mehl–Avrami equation [12]:

$$x(t) = 1 - \exp[-k(t - t_{\text{inc}})^n]$$

where  $x(t)$  is the normalized crystalline volume fraction relative to the asymptotic value for long-time annealing,  $k(T)$  the rate constant,  $n$  the Avrami exponent and  $t_{\text{inc}}$  the incubation time, i.e., the annealing time before the onset of crystallization. If the kinetics follows the Avrami law, a plot of  $\ln[-\ln(1 - x)]$  versus  $\ln(t - t_{\text{inc}})$  results in a straight line with slope  $n$ .

Table 1 displays the kinetic parameters obtained from fits with the Johnson–Mehl–Avrami equation for the  $\text{Fe}_{73.5}\text{Si}_{13.5}\text{B}_9\text{Cu}_1\text{Nb}_1\text{X}_2$  ( $X = \text{V}, \text{Mo}, \text{Nb}$  and  $\text{Zr}$ ) annealed alloys.

As expected, the incubation time ( $t_{\text{inc}}$ ) decreases and the rate constant ( $k$ ) increases with the annealing temperature. The values of the Avrami exponent are close to 1 for the studied alloys, in agreement with those previously reported for Finemet alloys [8,13]. Similar values are also found for Hitperm-type ( $\text{FeCoNbBCu}$ ) alloys [14], whereas exponents ranging between 1.8 and 2.2 have been reported for Nanoperm-type ( $\text{FeZrB}$ ) alloys [15]. For all the alloys, the  $n$  values near to 1 are related to features of the crystallization mechanisms in those types of alloys and it may be attributed to: (i) a controlled diffusion process with a nucleation rate close to zero and/or (ii) the presence of Cu-clusters preceding to the nanocrystallization of the iron-silicate phase, as revealed by atom probe field ion microscopy (APFIM) [16] and extended X-ray absorption fine structure (EXAFS) spectroscopy [9,17], which reduce the stability of the Fe-rich

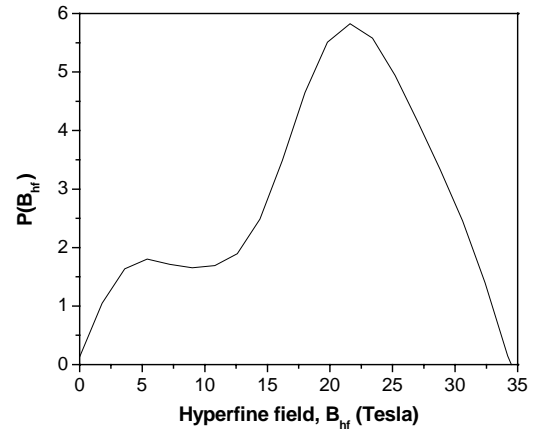


Fig. 5. Hyperfine field distribution curve that corresponds to the residual amorphous intergranular phase of the  $\text{Fe}_{73.5}\text{Si}_{13.5}\text{B}_9\text{Cu}_1\text{Nb}_1\text{Mo}_2$  annealed alloy obtained from Mössbauer spectra at 300 K.

regions acting as catalyzers of the crystallization of the iron-silicate nanophase. The presence of Cu-clusters has been also detected by APFIM in  $\text{FeCoNbBCu}$  alloys [18].

The diffusion velocity for the distinct atomic species is different and varies in a different way as the crystallization progresses. High contents of refractory element (like as Nb and B atoms) have been determined by APFIM at the periphery of crystalline grains in Finemet alloys [16]. Therefore, the cluster formation effect creates a diffusion barrier due to the segregation of the refractory elements (Nb, Zr, V and Mo) and B atoms, which are responsible for the inhibition of iron-silicate grain growth. Moreover, it can be expected that the segregation is one of the main phenomena responsible for the increase of the local activation energy [19,20]. In our case, the activation energy values were calculated to be roughly 3 eV, independent of the refractory-based alloys.

The presence of cluster formation in our samples can be explained based on the bimodal behavior of the hyperfine field distribution, corresponding to the residual amorphous intergranular phase shown in Fig. 5.

Thus, the two peaks observed in the hyperfine field distribution curve may be due to the presence of two magnetically distinct types of iron sites within the remaining amorphous phase: the high-field values can be attributed to the Fe atoms having preferentially Fe, B and Si atoms as nearest-neighbors, whereas the low-field component is ascribed to those surrounded by refractory elements. The growth of the iron-silicate crystallite is hindered by slowly diffusing inhibitors accumulating at the surface of the crystallite.

#### 4. Conclusions

Time dependent in situ isothermal Mössbauer experiments have been performed at several temperatures in order to study the kinetics of the nanocrystallization process of the  $\text{FeSiBCuNbX}$  ( $X = \text{Zr}, \text{Nb}, \text{Mo}$  and  $\text{V}$ ) amorphous alloys. This process was followed by measuring the relative

absorption Mössbauer area as a function of the annealing time, for the crystalline component associated with a  $\text{DO}_3$  structure iron-silicate phase, with respect to the area of the subspectrum attributed to the intergranular amorphous matrix. The nanocrystalline fraction increases monotonically with increasing annealing time up to a saturation value. For the studied alloys, the volume fraction of the iron-silicate nanocrystalline phase, obtained under similar annealing conditions, increases in the sequence  $\text{Zr} < \text{Nb} < \text{Mo} < \text{V}$ . The nanocrystallization kinetics is described using the Johnson–Mehl–Avrami approach and values close to 1 were found for the Avrami exponent for all alloys. The  $n$  values close to 1 are related to an increase of a diffusion barrier, suggesting a controlled diffusion process with a nucleation rate close to zero. The activation energy was found to be approximately 3 eV.

### Acknowledgements

The authors are indebted to the group of Prof. Dr. A. Conde for sample supplies. This work was partially supported by the CONCYTEC of the Peruvian Government, by CNPq (PCI-program) of the Brazilian Government and by the Latin American Center of Physics. E. Baggio-Saitovitch thanks FAPERJ for the support as Cientista do Nosso Estado.

### References

- [1] Y. Yoshizawa, S. Oguma, K. Yamauchi, *J. Appl. Phys.* 64 (1988) 6044.
- [2] G. Herzer, *J. Magn. Magn. Mater.* 192 (1992) 258.
- [3] U. Köster, U. Schünemann, M. Blank-Bewersdorff, K. Brauer, M. Sutton, G.B. Stephenson, *Mater. Sci. Eng. A* 133 (1991) 611.
- [4] P. Duhaj, P. Svec, D. Janickovic, I. Matko, M. Hlasnik, *Mater. Sci. Eng. B* 14 (1992) 357.
- [5] J.M. Borrego, A. Conde, V.A. Peña-Rodríguez, J.M. Greneche, *Hyp. Interact.* 131 (2000) 67.
- [6] J.M. Borrego, C.F. Conde, A. Conde, *Philos. Magn. Lett.* 80 (2000) 359.
- [7] J.M. Borrego, A. Conde, *Mater. Sci. Eng. A* 226–228 (1997) 663.
- [8] J.M. Borrego, C.F. Conde, M. Millán, A. Conde, M.J. Capitán, J.L. Joulaud, *Nanostruct. Mater.* 10 (1998) 275.
- [9] J.M. Borrego, C.F. Conde, A. Conde, A.V. Chadwick, G. Morrison, *J. Non-Cryst. Solids* 352 (1998) 232.
- [10] R.A. Brand, J. Lauer, D.M. Herlach, *J. Phys. F: Met. Phys.* 12 (1983) 675.
- [11] I. Vincze, *Solid State Commun.* 25 (1978) 689.
- [12] M. Avrami, *J. Chem. Phys.* 9 (1941) 177.
- [13] C.F. Conde, A. Conde, *Mater. Lett.* 21 (1994) 409.
- [14] J.S. Blázquez, C.F. Conde, A. Conde, *J. Non-Cryst. Solids* 287 (2001) 187.
- [15] K. Suzuki, A. Makino, A.P. Tsai, A. Inoue, T. Masumoto, *Mater. Sci. Eng. A* 179–180 (1994) 501.
- [16] K. Hono, K. Hiraga, Q. Wang, A. Inoue, T. Sakurai, *Acta Metall. Mater.* 40 (1992) 2137.
- [17] J.D. Ayers, V.G. Harris, J.A. Sprague, W.T. Elam, *IEEE Trans. Magn.* 29 (1993) 2664.
- [18] Y. Zhang, J.S. Blázquez, A. Conde, P.J. Warren, A. Cerezo, *Mater. Sci. Eng. A* 353 (2003) 158–163.
- [19] I. Matko, P. Duhaj, P. Svec, D. Janickovic, *Mater. Sci. Eng. A* 179–180 (1994) 557.
- [20] T. Liu, N. Chen, Z.X. Xu, R.Z. Ma, *J. Magn. Magn. Mater.* 152 (1996) 359.